

Influence of mixed convection on blood flow of Jeffrey fluid through a tapered stenosed artery

Noreen Sher Akbar¹, T. Hayat^{1,2}, S. Nadeem¹ and Awatif A. Hendi²

¹ Department of Mathematics, Quaid-i-Azam University 45320, Islamabad 44000 Pakistan

² Department of Physics, Faculty of Science, King Saud University, P.O.Box 1846, Riyadh 11321, Saudi Arabia

Abstract: Effect of heat and mass transfer on the blood flow through a tapered artery with stenosis is examined assuming blood as Jeffrey fluid. The governing equations have been modelled in cylindrical coordinates. Series solutions are constructed for the velocity, temperature, concentration, resistance impedance, wall shear stress and shearing stress at the stenosis throat. Attention has been mainly focused to the analysis of embedded parameters in converging, diverging and non-tapered situations.

Keywords: Jeffrey fluid, blood flow, mixed convection.

1. Introduction

The non-planer arterial configuration is associated closely with swirling blood flow. Arteries (as a living tissues) require a supply of metabolites including oxygen and removal of waste products. Blood is multi-component mixtures, consisting of plasma, red and white blood cells (RBCs and WBCs), platelets, etc [1]. The analysis of blood flow in arteries is very popular now a days because of some cardiovascular diseases [2,3]. The nature of blood itself sometimes has a key role in such diseases. No doubt, it is concluded now that blood is a non-Newtonian fluid at low shear rate (100/s). Humphrey [2, p.357] pointed out that a rheological properties of blood greatly depends upon the change in flow configuration. He characterized blood as a mixture (i.e solid and fluid). Further Thurston and Chien et al. [4,5] experimentally observed viscoelastic properties of blood. Jones [6] found that the flow behaviour of blood changes from Newtonian to non-Newtonian character when there is a change in the diameter of vessel from large arteries to small branches and capillaries. The flow varies with typical Reynold number from small arteries to large arteries. Siddiqui et al. [7] examined the rheological effects on pulsatile flow of blood in a stenosed artery. Mekheimer and El Kot [8] presented micropolar fluid model for axisymmetric blood flow through an axially nonsymmetric but radially symmetric mild stenosis tapered artery. Unsteady flow analysis for blood as non-Newtonian fluid through tapered arteries with a stenosis is studied numerically by Mandal [9]. Varshney et al [10] considered the generalized power law fluid model for blood flow in an artery having multiple stenosis. They carried out the numerical study under the action of transverse magnetic field. Power law fluid model for blood flow through a tapered artery with a stenosis is recently developed by Nadeem et al. [11]. In another article, Nadeem and Akram [12] revisited the flow analysis of ref. [11] for Jeffrey fluid. Mustafa et al. [13] presented the numerical simulation of generalized Newtonian blood flow through a couple of irregular arterial stenosis. The blood flow with an irregular stenosis in presence of magnetic field has been looked at Abdullah et al. [14]. It is noted from existing literature that only few attempts investigate the blood flow in presence

¹Corresponding author: E-mail: noreensher@yahoo.com.(Noreen Sher Akbar)

of heat and mass transfer. Influence of pulsatile blood flow and heating scheme on the temperature distribution with reference to hyperthermia treatment was studied by Khanafer et al. [15]. Unsteady flow and mass transfer in models of stenotic arteries considering fluid-structure interaction was simulated by Valencia and Villanueva [16]. Back et al [17] examined the flow field and mass transfer analysis in arteries with longitudinal ridges. Heat and mass transfer in a separated flow region for high Prandtl and Schmidt numbers have been studied by Ma et al. [18]. Akbar and Nadeem [19] constructed the simulation of heat and chemical reactions for Reiner Rivlin fluid model of blood flow through a tapered artery subject to a stenosis. Recently Nadeem and Akbar [20] studied the blood flow for Walter's B fluid model through a tapered artery with heat and mass transfer. Some important article related to the topic are included in Refs. [22-26]. The interest in the present article is to analyze the effects of mixed convection blood flow of Jeffery through a tapered stenoid artery. Analysis has been carried out in the presence of heat and mass transfer. We arranged this article in the following fashion. The next section consists of mathematical formulation. The solution expressions for velocity, temperature, concentration, resistance impedance, wall shear stress and shearing stress at the stenosis throat are constructed in section three. Section four analyzes the salient features of the problem by graphically illustration.

2. Problem development

We examine incompressible flow of Jeffrey fluid with constant viscosity μ and density ρ in a tube having length L . The cylindrical coordinate system (r, θ, z) is chosen such that \bar{u} and \bar{w} are the velocity components in the \bar{r} and \bar{z} directions respectively. Here $r=0$ is selected the axis of the symmetry of the tubes. Mixed convection is considered in the presence of heat and mass transfer by assigning the temperature \bar{T}_0 and concentration \bar{C}_0 to the wall of the tube. Symmetry condition for both temperature and concentration is employed at the centre of the tube. The consideration of stenosis is represented as [8] :

$$h(z) = d(z) \left[1 - \eta_1 \left(b^{n-1} (z-a) - (z-a)^n \right) \right],$$

$$a \leq z \leq a+b,$$

$$= d(z), \text{ otherwise} \quad 1$$

with

$$d(z) = d_0 + \xi z. \quad 2$$

In above equations $d(z)$ is the radius of the tapered arterial segment in the stenotic region, d_0 is the radius of the non-tapered artery in the non-stenotic region, ξ is the tapering parameter, b is the length of stenosis, $(n \geq 2)$ is a parameter determining the shape of the constriction profile and referred to as the shape parameter the symmetric stenosis occurs for $n=2$ and a indicates its location (see in Fig. 1).

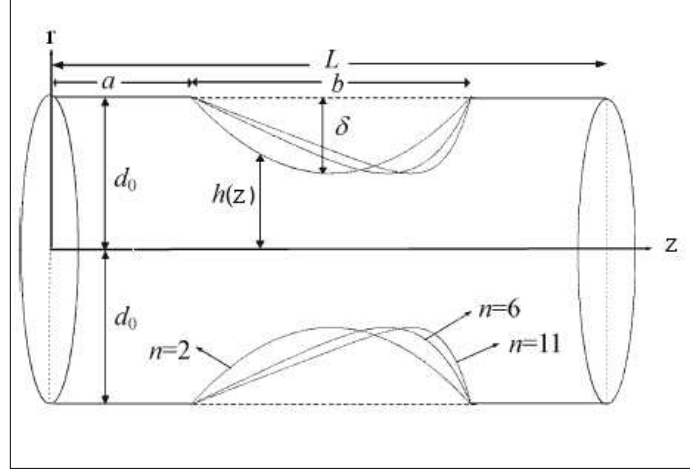


Fig. 1. Geometry of an axially nonsymmetrical stenosis in the artery. The parameter η is given by

$$\eta = \frac{\delta^* n^{\frac{n}{n-1}}}{d_0 b^n (n-1)},$$

in which maximum height of stenosis located at $z = a + \frac{b}{n^{\frac{n}{n-1}}}$ is in ref. [8]

The equations governing the flow are

$$\frac{\partial \bar{u}}{\partial \bar{r}} + \frac{\bar{u}}{\bar{r}} + \frac{\partial \bar{w}}{\partial \bar{z}} = 0, \quad 3$$

$$\rho \left(\bar{u} \frac{\partial}{\partial \bar{r}} + \bar{w} \frac{\partial}{\partial \bar{z}} \right) \bar{u} = -\frac{\partial \bar{p}}{\partial \bar{r}} + \frac{1}{\bar{r}} \frac{\partial}{\partial \bar{r}} (\bar{r} \bar{\mathbf{S}}_{rr}) + \frac{\partial}{\partial \bar{z}} (\bar{\mathbf{S}}_{rz}) - \frac{\bar{\mathbf{S}}_{\theta\theta}}{\bar{r}}, \quad 4$$

$$\rho \left(\bar{u} \frac{\partial}{\partial \bar{r}} + \bar{w} \frac{\partial}{\partial \bar{z}} \right) \bar{w} = -\frac{\partial \bar{p}}{\partial \bar{z}} + \frac{1}{\bar{r}} \frac{\partial}{\partial \bar{r}} (\bar{r} \bar{\mathbf{S}}_{rz}) + \frac{\partial}{\partial \bar{z}} (\bar{\mathbf{S}}_{zz}) + \rho g \alpha (\bar{T} - \bar{T}_0) + \rho g \alpha (\bar{C} - \bar{C}_0), \quad 5$$

$$\begin{aligned} \rho c_p \left(\bar{u} \frac{\partial}{\partial \bar{r}} + \bar{w} \frac{\partial}{\partial \bar{z}} \right) \bar{T} &= \bar{\mathbf{S}}_{rr} \frac{\partial \bar{u}}{\partial \bar{r}} + \bar{\mathbf{S}}_{rz} \frac{\partial \bar{w}}{\partial \bar{r}} + \bar{\mathbf{S}}_{rz} \frac{\partial \bar{u}}{\partial \bar{z}} + \bar{\mathbf{S}}_{zz} \frac{\partial \bar{w}}{\partial \bar{z}} \\ &+ k \left(\frac{\partial^2 \bar{T}}{\partial \bar{r}^2} + \frac{1}{\bar{r}} \frac{\partial \bar{T}}{\partial \bar{r}} + \frac{\partial^2 \bar{T}}{\partial \bar{z}^2} \right), \end{aligned} \quad 6$$

$$\begin{aligned} \left(\bar{u} \frac{\partial}{\partial \bar{r}} + \bar{w} \frac{\partial}{\partial \bar{z}} \right) \bar{C} &= D \left(\frac{\partial^2 \bar{C}}{\partial \bar{r}^2} + \frac{1}{\bar{r}} \frac{\partial \bar{C}}{\partial \bar{r}} + \frac{\partial^2 \bar{C}}{\partial \bar{z}^2} \right) \\ &+ \frac{DK_T}{T_m} \left(\frac{\partial^2 \bar{T}}{\partial \bar{r}^2} + \frac{1}{\bar{r}} \frac{\partial \bar{T}}{\partial \bar{r}} + \frac{\partial^2 \bar{T}}{\partial \bar{z}^2} \right), \end{aligned} \quad 7$$

where \bar{p} is the pressure, \bar{T} is the temperature, \bar{C} is the concentration of fluid, λ is the density, k denotes the thermal conductivity, c_p is the specific heat at constant pressure, T_m is the temperature of the medium, D is the coefficient of mass diffusivity, K_T is the thermal-diffusion ratio and g is due to the gravity.

Extra stress tensor $\bar{\mathbf{S}}$ in Jeffrey fluid is [12]

$$\bar{\mathbf{S}} = \frac{\mu}{1 + \lambda_1} (\dot{\boldsymbol{\gamma}} + \lambda_2^* \ddot{\boldsymbol{\gamma}}), \quad 8$$

where μ is the viscosity, λ_1 is the ratio of relaxation to retardation times, $\dot{\boldsymbol{\gamma}}$ is the shear rate and λ_2^* the retardation time. Defining

$$\begin{aligned} r &= \frac{\bar{r}}{d_0}, \quad z = \frac{\bar{z}}{b}, \quad w = \frac{\bar{w}}{u_0}, \quad u = \frac{b\bar{u}}{u_0\delta}, \quad p = \frac{d_0^2\bar{p}}{u_0b\mu}, \quad h = \frac{\bar{h}}{d_0}, \\ \text{Re} &= \frac{\rho bu_0}{\mu}, \quad S_{rr} = \frac{b\bar{\mathbf{S}}_{rr}}{u_0\mu}, \quad \tilde{S}_{rz} = \frac{d_0\bar{\mathbf{S}}_{rz}}{u_0\mu}, \quad S_{zz} = \frac{b\bar{\mathbf{S}}_{zz}}{u_0\mu}, \quad S_{\theta\theta} = \frac{b\bar{\mathbf{S}}_{\theta\theta}}{u_0\mu}, \\ \lambda_2 &= \frac{\lambda_2^*u_0}{b}, \quad \theta = \frac{\bar{T} - \bar{T}_0}{\bar{T}_0}, \quad E_c = \frac{u_0^2}{c_p\bar{T}_0}, \quad \text{Pr} = \frac{c_p\mu}{k}, \quad C_r = \frac{g\alpha d_0^3\bar{C}_0}{\nu^2}, \\ S_r &= \frac{\rho DK_T\bar{T}_0}{\mu T_m\bar{C}_0}, \quad S_c = \frac{\mu}{D\rho}, \quad \sigma = \frac{(\bar{C} - \bar{C}_0)}{\bar{C}_0}, \quad G_r = \frac{g\alpha d_0^3\bar{T}_0}{\nu^2}, \end{aligned} \quad 9$$

where S_r is the Soret number, S_c is Schmidt number, P_r is the Prandtl number, E_c is the Eckert number, ν is the kinematic viscosity, μ is the dynamic viscosity, u_0 is the velocity averaged over the section of the tube of the width d_0 and σ is the concentration, and using Eqs. (6) and (9) along with the additional conditions [8] :

$$(i) \frac{\text{Re} \delta^n n^{\left(\frac{1}{n-1}\right)}}{b} \ll 1, \quad 10a$$

$$(ii) \frac{d_0 n^{\left(\frac{1}{n-1}\right)}}{b} \sim O(1), \quad 10b$$

we have for mild stenosis $\left(\frac{\delta^*}{d_0} \ll 1\right)$ the following expressions

$$\frac{\partial u}{\partial r} + \frac{u}{r} + \frac{\partial w}{\partial z} = 0, \quad 11$$

$$\frac{\partial p}{\partial r} = 0, \quad 12$$

$$\frac{\partial p}{\partial z} = \frac{1}{r} \frac{\partial}{\partial r} \left(\frac{r}{1 + \lambda_1} \left\{ \left(\frac{\partial w}{\partial r} \right) + \lambda_2 w \left(\frac{\partial^2 w}{\partial r \partial z} \right) \right\} \right) + G_r \theta + C_r \sigma. \quad 13$$

$$\frac{1}{r} \frac{\partial}{\partial r} \left(r \frac{\partial \theta}{\partial r} \right) + B_r \left(\frac{1}{1 + \lambda_1} \left\{ \left(\frac{\partial w}{\partial r} \right)^2 + \lambda_2 w \left(\frac{\partial^2 w}{\partial r \partial z} \right) \left(\frac{\partial w}{\partial r} \right) \right\} \right) = 0, \quad 14$$

$$\frac{1}{S_c} \left(\frac{1}{r} \frac{\partial}{\partial r} \left(r \frac{\partial \sigma}{\partial r} \right) \right) + S_r \left(\frac{1}{r} \frac{\partial}{\partial r} \left(r \frac{\partial \theta}{\partial r} \right) \right) = 0, \quad 15$$

where the Brinkman number $B_r = E_c \text{Pr}$. The boundary conditions are now given by

$$\frac{\partial w}{\partial r} = 0, \quad \frac{\partial \theta}{\partial r} = 0, \quad \frac{\partial \sigma}{\partial r} = 0 \quad \text{at } r = 0, \quad 16a$$

$$w = 0, \quad \theta = 0, \quad \sigma = 0 \quad \text{at } r = h(z), \quad 16b$$

$$h(z) = (1 + \xi z) \left[1 - \eta_1 \left((z - \sigma_1) - (z - \sigma_1)^n \right) \right], \quad 17$$

$$\sigma_1 \leq z \leq \sigma_1 + 1,$$

and

$$\eta_1 = \frac{\delta n^{\frac{n}{n-1}}}{(n-1)}, \quad \delta = \frac{\delta^*}{d_0}, \quad \sigma_1 = \frac{a}{b}, \quad \xi' = \frac{\xi b}{d_0}, \quad \xi = \tan \phi \quad 18$$

in which ϕ is called tapered angle. Further, for converging tapering or ($\phi < 0$), non-tapered artery ($\phi = 0$) and the diverging tapering ($\phi > 0$).

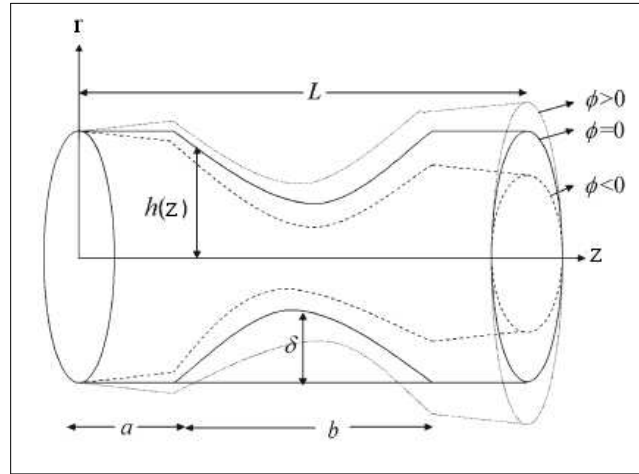


Fig. 2. Geometry of the axially stenosed tapered artery.

3. Solution of the problem

We have an interest to compute the series solution by homotopy perturbation method [21]. For that we write

$$H(q, w) = (1-q)[L(w) - L(w_{10})] + q \left[L(w) - \frac{\partial p}{\partial z} (1 + \lambda_1) - \lambda_2 (1 + \lambda_1) w \left(\frac{\partial^2 w}{\partial r \partial z} \right) + G_r (1 + \lambda_1) \theta + C_r (1 + \lambda_1) \sigma \right], \quad 19$$

$$H(q, \theta) = (1-q)[L(\theta) - L(\theta_{10})] + q \left[L(\theta) + B_r \left(\frac{1}{1 + \lambda_1} \left\{ \left(\frac{\partial w}{\partial r} \right)^2 + \lambda_2 w \left(\frac{\partial^2 w}{\partial r \partial z} \right) \left(\frac{\partial w}{\partial r} \right) \right\} \right) \right], \quad 20$$

$$H(q, \sigma) = (1-q)[L(\sigma) - L(\sigma_{10})] + q \left[L(\sigma) + S_r S_c \left(\frac{1}{r} \frac{\partial}{\partial r} \left(r \frac{\partial \theta}{\partial r} \right) \right) \right], \quad 21$$

and choose $L = \frac{1}{r} \frac{\partial}{\partial r} \left(r \frac{\partial}{\partial r} \right)$ as the auxiliary linear operator. Further the initial guesses are represented by

$$w_{10}(r, z) = \frac{\partial p_0}{\partial z} \left(\frac{r^2 - h^2}{4} \right), \quad \theta_{10}(r, z) = \left(\frac{r^2 - h^2}{4} \right), \quad \sigma_{10}(r, z) = - \left(\frac{r^2 - h^2}{4} \right). \quad 22$$

Putting

$$w(r, q) = w_0 + qw_1 + q^2 w_2 + \dots \quad 23$$

$$\theta(r, q) = \theta_0 + q\theta_1 + q^2 \theta_2 + \dots \quad 24$$

$$\sigma(r, q) = \sigma_0 + q\sigma_1 + q^2 \sigma_2 + \dots \quad 25$$

and then employing the procedure of ref. [19] for $q = 1$, we have the following results for velocity, temperature and concentration fields:

$$w(r, z) = \left(\frac{r^2 - h^2}{4} \right) (1 + \lambda_1) \frac{\partial p}{\partial z} + a_2 (r^2 - h^2) + a_3 (r^3 - h^3) + a_4 (r^4 - h^4) + a_{23} (r^8 - h^8) + a_{24} (r^7 - h^7) + a_{25} (r^6 - h^6) + a_{26} (r^5 - h^5) + a_{27} (r^4 - h^4) + a_{28} (r^3 - h^3) + a_{29} (r^2 - h^2), \quad 26$$

$$\theta(r, z) = a_5 (r^4 - h^4) + a_6 (r^6 - h^6) + a_{51} (r^{11} - h^{11}) + a_{52} (r^8 - h^8) + a_{53} (r^7 - h^7) + a_{54} (r^6 - h^6) + a_{55} (r^5 - h^5) + a_{56} (r^4 - h^4) + a_{57} (r^3 - h^3), \quad 27$$

$$\begin{aligned}\sigma(r, z) = & -\left(\frac{r^2 - h^2}{4}\right) - S_r S_c (a_5(r^4 - h^4) + a_6(r^6 - h^6) + a_{51}(r^{11} - h^{11}) \\ & + a_{52}(r^8 - h^8) + a_{53}(r^7 - h^7) + a_{54}(r^6 - h^6) + a_{55}(r^5 - h^5) \\ & + a_{56}(r^4 - h^4) + a_{57}(r^3 - h^3)).\end{aligned}\quad 28$$

The volume flow rate Q is expressed as

$$Q = \int_0^h r w dr. \quad 29$$

Through Eqs. (26) and (29) one has

$$\frac{dp}{dz} = -\frac{16Q}{(1 + \lambda_1)h^4} + \frac{16a_{58}}{(1 + \lambda_1)h^4}. \quad 30$$

The pressure drop ($\Delta p = p$ at $z = 0$ and $\Delta p = -p$ at $z = L$) across the stenosis between the section $z = 0$ and $z = L$ can be obtained using the expression given below

$$\Delta p = \int_0^L \left(-\frac{dp}{dz}\right) dz, \quad 31$$

3.1. Resistance impedance

The resistance impedance is given by

$$\tilde{\lambda} = \frac{\Delta p}{Q} = \left\{ \int_0^a F(z) \Big|_{h=1} dz + \int_a^{a+b} F(z) dz + \int_{a+b}^L F(z) \Big|_{h=1} dz \right\}, \quad 32$$

in which

$$F(z) = \frac{16}{(1 + \lambda_1)h^4} - \frac{16a_{58}}{Q(1 + \lambda_1)h^4}.$$

On simplification, Eq. (32) yields

$$\tilde{\lambda} = \left\{ (L - b) \left(\frac{16}{(1 + \lambda_1)} - \frac{16a_{58}}{Q(1 + \lambda_1)} \right) + \int_a^{a+b} F(z) dz \right\}. \quad 33$$

3.2. Expression for the wall shear stress

The expression for dimensionless shear stress is

$$\tilde{\mathbf{S}}_{rz} = \left[\frac{1}{1 + \lambda_1} \left\{ \left(\frac{\partial w}{\partial r} \right) + \lambda_2 w \left(\frac{\partial^2 w}{\partial r \partial z} \right) \right\} \right]. \quad 34$$

The wall shear stress is of the form

$$\tilde{\mathbf{S}}_{rz} = \left[\frac{1}{1 + \lambda_1} \left\{ \left(\frac{\partial w}{\partial r} \right) + \lambda_2 w \left(\frac{\partial^2 w}{\partial r \partial z} \right) \right\} \right]_{r=h}. \quad 35$$

The shearing stress at the stenosis throat i.e the wall shear at the maximum height of the stenosis located at $z = \frac{a}{b} + \frac{1}{\frac{a}{n} - 1}$ can be expressed as

$$\tilde{\tau}_s = \tilde{\mathbf{S}}_{rz} \Big|_{h=1-\delta}.$$

The final expressions for the dimensionless resistance to λ , wall shear stress \mathbf{S}_{rz} and the shearing stress at the throat τ_s are

$$\lambda = \frac{\bar{\lambda}}{\lambda_0} = \frac{1}{3} \left\{ \left(1 - \frac{b}{L} \right) \left(\frac{16}{(1+\lambda_1)} - \frac{16a_{58}}{Q(1+\lambda_1)} \right) + \frac{1}{L} \int_a^{a+b} R(z) dz \right\}, \quad 37$$

$$\tau_{rz} = \frac{\tilde{S}_{rz}}{\tau_0}, \quad \tau_s = \frac{\tilde{\tau}_s}{\tau_0}, \quad 38$$

with

$$\lambda_0 = 3L, \quad \tau_0 = 4Q. \quad 39$$

4. Numerical results and discussion

Our interest in this section is to analyze the effects of the ratio of relaxation to retardation time λ_1 , retardation time λ_2 , the stenosis shape n and maximum height of the stenosis δ for converging tapering, diverging and non-tapered arteries in Jeffrey fluid. This object has been achieved through the plots (3) to (11). The variation of axial velocity for λ_1 , n , λ_2 and δ in converging, diverging and non-tapered arteries are displayed in the Figs. (3a) to (3d). We observed that due to increase in λ_1 , n and δ , the velocity profile decreases. The velocity increases due to increase in λ_2 . It is also seen that for the case of converging tapering the velocity gives larger values as compared to the case of diverging tapering and non-tapered arteries. Figs (4a) to (4c) show how the converging, diverging and non-tapered arteries influence on the wall shear stress τ_{rz} . Interestingly with an increase in λ_1 and δ the shear stress increases and decreases with an increase in λ_2 . It is also seen that the stress yield diverging tapering with tapered angle $\phi > 0$, converging tapering with tapered angle $\phi < 0$ and non-tapered artery with tapered angle $\phi = 0$. In the Figs. (5a) and (5b) it has been noticed that the impedance resistance increases for converging, diverging and non-tapered arteries when we increase λ_1 . Such resistance decreases upon increasing λ_2 . We also observed that resistive impedance in a diverging tapering appear to be smaller than in converging tapering because the flow rate is higher in the former case when compared with the later. Impedance resistance attains its maximum values in the symmetric stenosis case ($n = 2$). Figs. (6a) and (6b) illustrate the variation of shearing stress at the stenosis throat τ_s with δ . The shearing stress at the stenosis throat decreases with an increase in Q and λ_1 . Figs. (7a) and (7b) depict the variation of temperature profile for different values of Brinkman number B_r and ratio of relaxation to retardation time λ_1 . It is observed that with an increase in Brinkman number B_r . The temperature profile decreases while increases with an increase in ratio of relaxation to retardation time λ_1 , temperature profile has the large values for converging tapering when compared with the diverging and non-tapered arteries. Figs. (8a) and (8b) are prepared to see the variation of concentration profile for Brinkman number B_r , ratio of

relaxation to retardation time, λ_1 and Soret number S_r . It is found that with an increase in Brinkman number B_r and Soret number S_r , the concentration profile increases. However it decreases because of an increase in ratio of relaxation to retardation time λ_1 . It is also observed that concentration profile has an opposite behavior as compared to the temperature profile. Figs. (9) to (11) show the streamlines for different values of n , λ_1 and λ_2 . Streamlines for different values of the stenosis shape n is shown in Fig. (9). Here it is noticed that the size of the trapping bolus increases when we increase the stenosis shape. Figs. (10) and (11) are plotted to see the streamlines for different values of ratio of relaxation to retardation time λ_1 and retardation time λ_2 . Here the size of the trapping bolus increases with an increase in ratio of relaxation to retardation time while it decreases when retardation time increases.

Fig. 3 . Variation of velocity profile for (a) $\lambda_1 = 0.3, n = 2$ and $\lambda_2 = 0.5$, (b) $\lambda_1 = 0.3, n = 2$ and $\delta = 0.5$, (c) $\lambda_1 = 0.3, \lambda_2 = 0.5$ and $\delta = 0.5$. The other parameters are $B_r = 0.3, \sigma_1 = 0.0, z = 0.5, Q = 0.3, G_r = 0.5, C_r = 0.3, S_c = 0.5$ and $S_r = 0.5$.

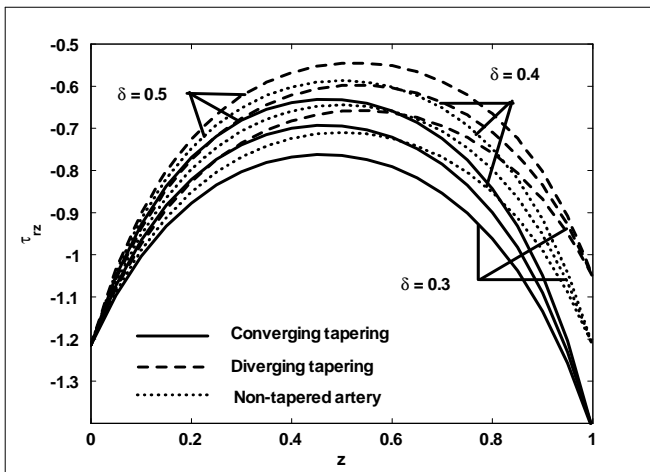


Fig.4(a)

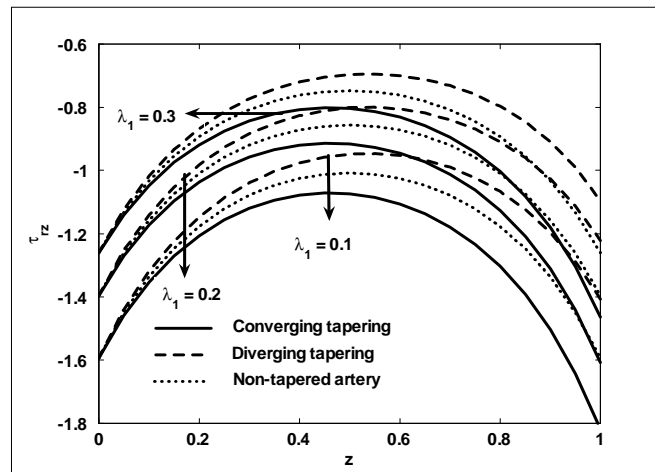


Fig.4(b)

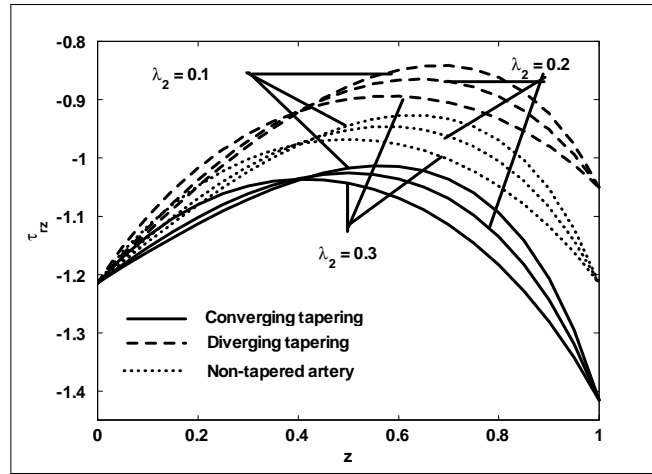


Fig.4

Fig. 4 . Variation of wall shear stress for (a) $\lambda_1 = 0.3$ and $\lambda_2 = 0.5$, (b) $\lambda_1 = 0.3$ and $\delta = 0.5$, (c) $\lambda_1 = 0.3$ and $\delta = 0.5$. The other parameters are $B_r = 0.3$, $\sigma_1 = 0.0$, $z = 0.5$, $n = 2$, $Q = 0.3$, $G_r = 0.5$, $C_r = 0.3$, $S_c = 0.5$ and $S_r = 0.5$.

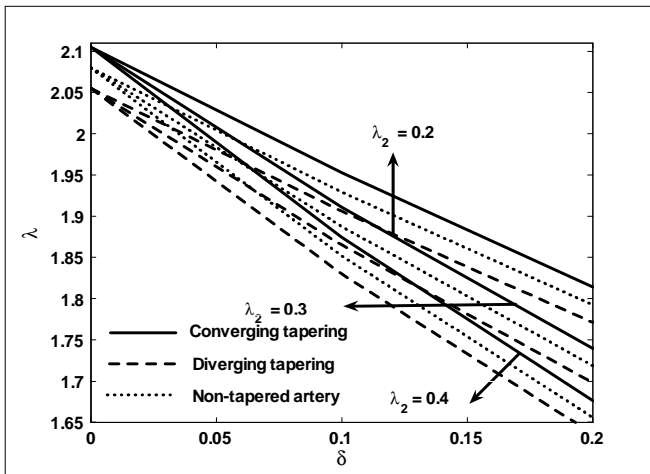


Fig.5(a)

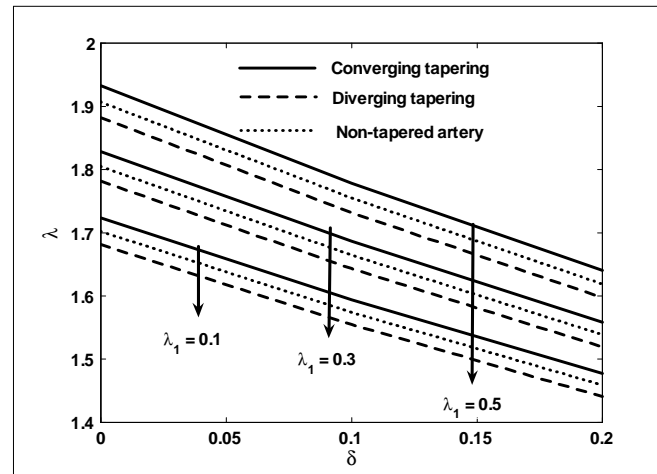


Fig.5(b)

Fig. 5 . Variation of resistance for (a) $\lambda_1 = 0.3$, (b) $\lambda_2 = 0.4$. The other parameters are $Q = 0.3$, $L = 1$, $\sigma_1 = 0.0$, $B_r = 0.5$, $z = 0.5$, $G_r = 0.5$, $C_r = 0.3$, $S_c = 0.5$ and $S_r = 0.5$.

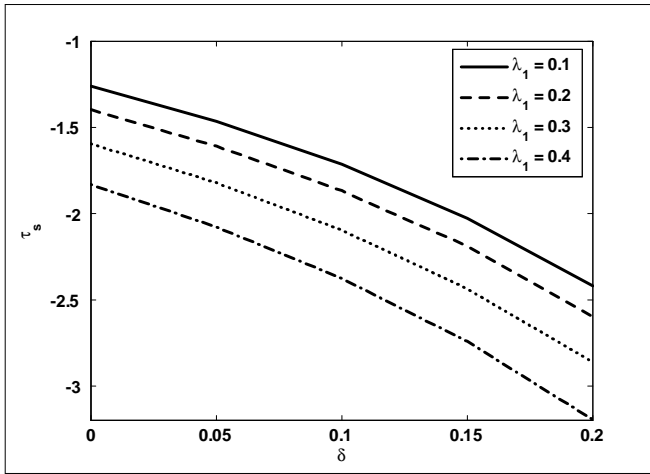


Fig.6

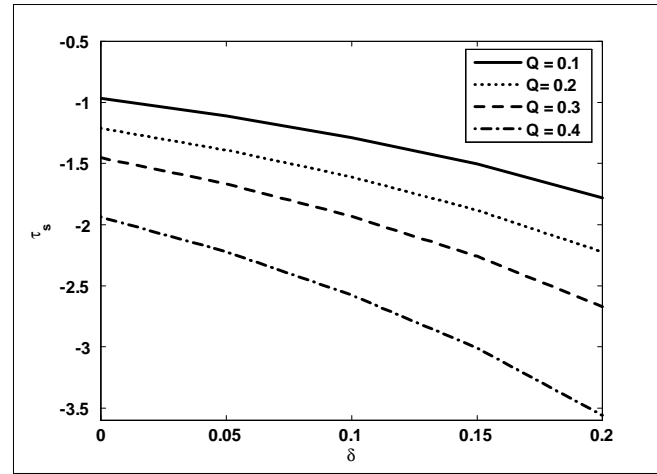


Fig.6

Fig. 6 . Variation of shear stress at the stenosis throat for (a) $Q=0.5$, (b) $\lambda_1=0.3$. The other parameters are $B_r=0.3$, $\sigma=0.0$, $z=0.5$, $n=2$, $\delta=0.3$, $G_r=0.5$, $C_r=0.3$, $S_c=0.5$, $S_r=0.5$ and $\lambda_2=0.3$.

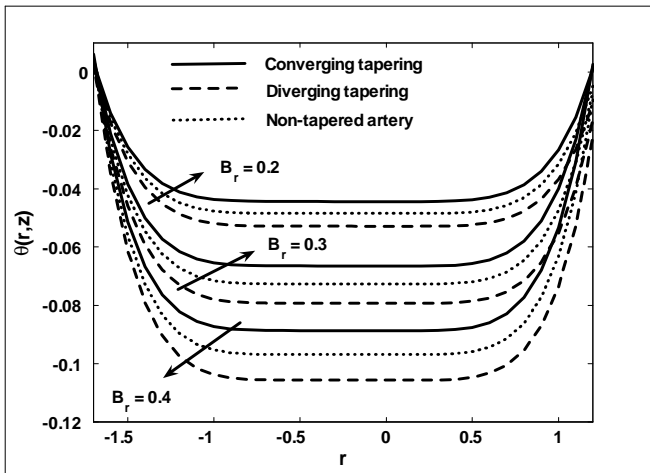


Fig.7

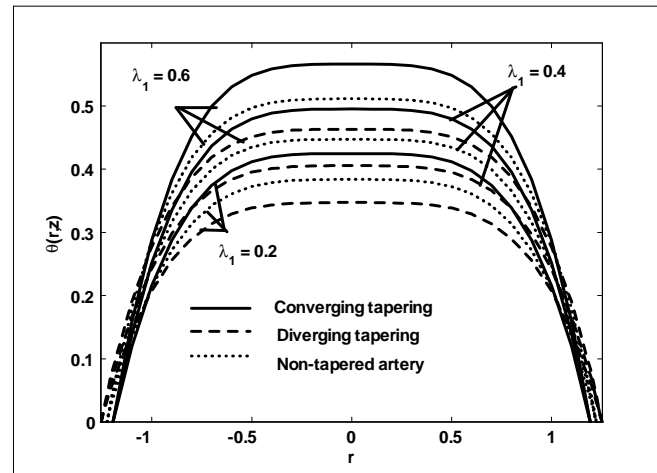


Fig.7

Fig. 7 . Variation of temperature profile for (a) $\lambda_1=0.5$, (b) $B_r=0.3$. The other parameters are $Q=0.3$, $\sigma=0.0$, $z=0.5$, $n=2$, $\delta=0.3$, $G_r=0.5$, $C_r=0.3$, $S_c=0.5$, $S_r=0.5$ and $\lambda_2=0.3$.

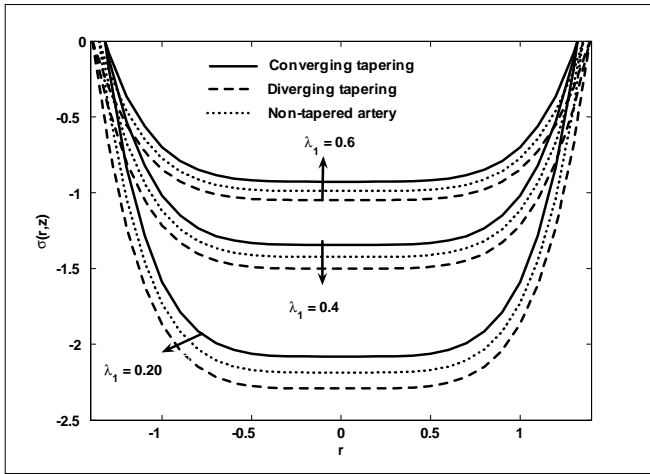


Fig.8

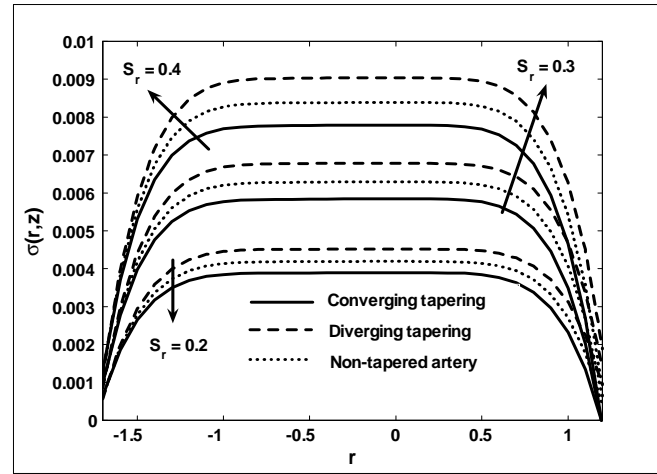


Fig.8

Fig. 8 . Variation of concentration profile for (a) $S_r = 0.5$, (b) $\lambda_1 = 0.3$. The other parameters are $Q = 0.3$, $\sigma = 0.0$, $z = 0.5$, $n = 2$, $\delta = 0.3$, $G_r = 0.5$, $C_r = 0.3$, $S_c = 0.5$ and $\lambda_2 = 0.3$.

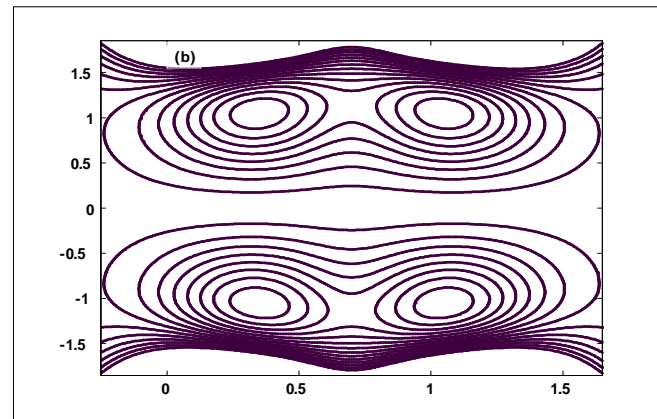
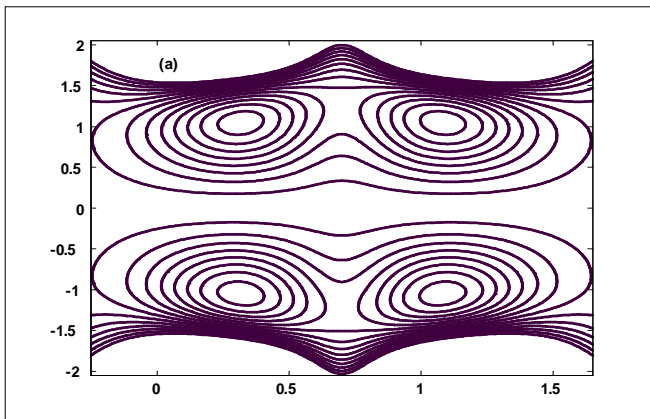


Fig. 9 . Streamlines for different values of n (a) $n = 2$ (b) $n = 4$. The other parameters are $Q = 0.3$, $\delta = 0.1$, $\lambda_1 = 0.2$, $G_r = 0.4$, $S_c = 0.5$, $S_r = 0.5$, $C_r = 0.6$ and $\lambda_2 = 0.3$.

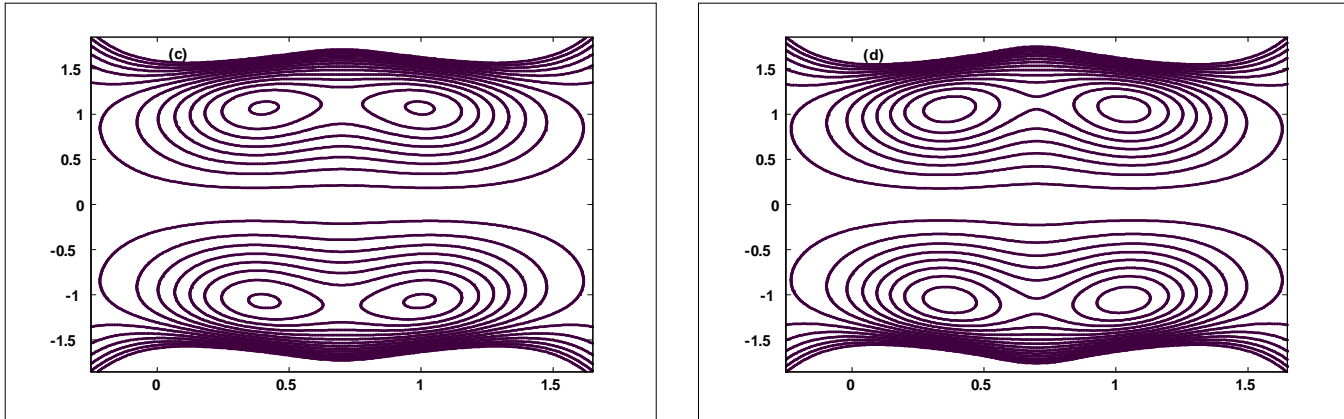


Fig. 10 . Streamlines for different values of λ_1 (c) $\lambda_1 = 0.1$ (d) $\lambda_1 = 0.3$. The other parameters are $Q = 0.3$, $\delta = 0.1$, $n = 2$, $G_r = 0.4$, $S_c = 0.5$, $S_r = 0.5$, $C_r = 0.6$ and $\lambda_2 = 0.3$.

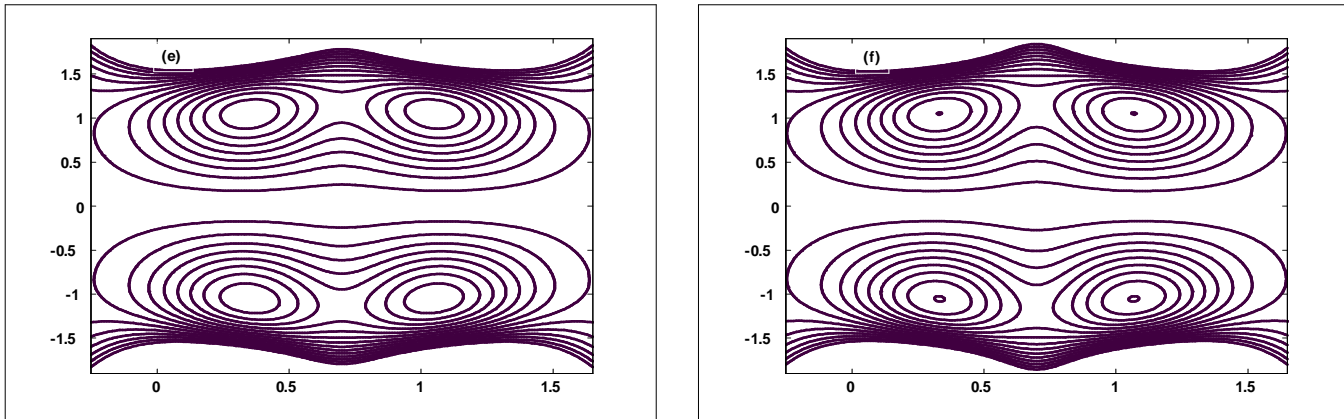


Fig. 11 . Streamlines for different values of λ_2 (e) $\lambda_2 = 0.1$ (f) $\lambda_2 = 0.3$. The other parameters are $Q = 0.3$, $\delta = 0.1$, $\lambda_1 = 0.2$, $G_r = 0.4$, $S_c = 0.5$, $S_r = 0.5$, $C_r = 0.6$ and $n = 2$.

Conclusions

This study examines the mixed convection effects on blood flow of Jeffrey through a tapered stenosed artery. The main points of the performed analysis are as follows.

- 1 . The influence of relaxation to retardation times λ_1 , shape of the stenosis n and height of the stenosis δ on the velocity profile is qualitatively similar.
2. The velocity profile increases when retardation time λ_2 increases .
- 3 . The velocity in converging tapering gives larger values when compared with the cases of diverging and non-tapered arteries.

- 4 . The resistive impedance in a diverging tapering is smaller than converging tapering .
- 5 . Shear stress increases by increasing λ_1 and δ . However the shear stress decreases with an increase in λ_2 .
- 6 . It is observed that with an increase in Brinkman number B_r , the temperature profile decreases. The temperature profile increases with an increase in ratio of relaxation to retardation times λ_1 .
- 7 . Concentration profile has an opposite behavior in comparison to the temperature profile.

Acknowledgment: T. Hayat as a visiting Professor recognizes the support of Global research Network for Computational Mathematics and King Saud University

References

- [1]. Massoudi, M. and Phuoc, T. X. Pulsatile flow of blood using a modified second-grade fluid model, *Comput , Math with Appl*, 2008, vol.56, pp.199-211.
- [2]. Humphrey, J.D. and Delange, S.L. *An Introduction to Biomechanics*, Springer Science + Business Media, Inc., New York, 2004.
- [3]. Eringen, A.C., Continuum theory of dense rigid suspension, *Rheol. Acta.* 1991, vol.30, pp. 23-32.
- [4]. Thurston, G.B. , Viscoelasticity of human blood, *Biophys. J*, 1972, vol.12, pp.1205-1217.
- [5]. Chien, S. , King, R.G. , Skalak, R. , Usami S. and Copley, A.L. Viscoelastic properties of human blood and red cell suspension, *Biorheology*, 1975, vol.12, pp. 341-346.
- [6]. Jones, R.T., Blood flow, *Ann. Rev. Fluid Mech*, 1969, vol.1, pp.223-244.
- [7]. Siddiqui, S.U. , Verma, N.K. , Mishra, S. and Gupta, R.S. , Mathematical modelling of pulsatile flow of Casson's fluid in arterial stenosis, *Appl. Math. Comput*, 2009, vol. 210, pp.1-10.
- [8]. Mekheimer Kh. S. and El Kot, M. A. , The micropolar fluid model for blood flow through a tapered artery with a stenosis, *Acta Mech Sin*, 2008, vol.24, pp.637-644.
- [9]. Mandal, P. K. , An unsteady analysis of non-Newtonian blood flow through tapered arteries with a stenosis, *Int. J. of Non-linear . Mech*, 2005, vol.40, pp.151-164.
- [10]. Varshney, G., Katiyar V.K. and Kumar, S. , Effect of magnetic field on the blood flow in artery having multiple stenosis: a numerical study, *Int. J. Eng. Sci. and Tech*, 2010, vol.2, pp. 67-82.
- [11]. Nadeem S. and Akbar, N. S., Hayat , T. and Hendi, Awatif A , Power law fluid model for blood flow through a tapered artery with a stenosis, *Appl. Math. Comput*, 2011, vol.217, pp. 7108-7116.
- [12]. Nadeem S. and Akbar, N. S., Jeffrey fluid model for blood flow through a tapered artery with a stenosis, *J. Mech. Medicine and Biology*, 2011, vol.11, pp. 529-545.
- [13]. Mustafa, N. , Mandal, P.K. , Abdullah, I., Amin, N.S. and Hayat, T., Numerical Simulation of generalized Newtonian blood flow past a couple of irregular arterial stenosis, *Numer.Meth.Partial Diff. Eqs.* 2011, Vol.27, pp.960-981.
- [14]. Abdullah, I. , Amin, N. S. and Hayat, T., Magnetohydrodynamic effects on blood flow through an irregular stenosis, *Int.J.Number.Method Fluids* DOI : 10.1002/ fld.2436.
- [15]. Khanafer, K. , Bull, J. L. , Pop , I. and Berguer, R. , Influence of pulsatile blood flow and heating scheme on the temperature distribution during hyperthermia treatment, *Int.J.*

Heat and Mass Transfer, 2007, vol. 50, pp.4883-4890.

[16]. Valencia, A. and Villanueva, M., Unsteady flow and mass transfer in models of stenotic arteries considering fluid-structure interaction, *Int. Comm. Heat Mass Transfer*, 2006, vol.33, pp. 966-975.

[17]. Back, L. H. , Crawford, D. W. and Barndt, R. , Flow field and mass transport analysis in arteries with longitudinal ridges, *J Appl Physiol*, 1976, vol.41 , pp.910-919.

[18]. Ma, P. , Li , X. and Ku, D.N. Heat and mass transfer in a separated flow region for high Prandtl and Schmidt numbers under pulsatile conditions. *Int J Heat Mass Transfer*, 1994, vol.37, pp.2723-2736.

[19]. Akbar, N. S. and Nadeem, S. , Simulation of heat and chemical reactions on Reiner Rivlin fluid model for blood flow through a tapered artery with a stenosis, *Heat Mass transfer*, 2010, vol.46, pp.531-539.

[20]. Nadeem, S. , Akbar, N. S. , Influence of heat and chemical reactions on Walter's B fluid model for blood flow through a tapered artery, *Taiwan Institute of Chemical Engineers*, 2011, vol.42, pp. 67-75.

[21]. He, J.H. Application of homotopy perturbation method to nonlinear wave equations, *Chaos, Solitons & Fractals* . 2005, vol.26, pp.695-700.

[22]. Ellahi, R. *Steady and unsteady flow for newtonian and non-Newtonian fluids: Basics, concepts and methods"*, Publisher, VDM Germany (2009).

[23]. Khan, Y., Wo. Qingbiao., Faraz, N and Yildirim., A. . The effects of variable viscosity and thermal conductivity on a thin film flow over a shrinking/stretching sheet, , *Comput. & Math. with Appl.* 2011, vol.61, pp.3391-3399.

[24]. Yildirim., A. . New Equations for Kinetic Analysis of Non-isothermal Thermogravimetry, *Asian. J. of Chem.*, 2008, vol.20, pp. 2057-2063.

[25]. Shan, P., Bohn, D., Ren, J., Surken, N. Parameter Survey of Thermally Highly Loaded, Porous and Cooled Multi-Layer Systems for Turbine Blades, *J. of Therm. Sci.*, 2007, Vol.12. pp. 181-185.

[26]. Kato, H., Taniguchi, H. , Matsuda, K., Funazaki, K. , Kato, D., and Pallot, G. Experimental and Numerical Investigation on Compressor Cascade Flows with Tip Clearance at a Low Reynolds Number Condition. *J. of Therm. Sci.*, 2011, Vol.20. pp. 481-485.